Hindawi Publishing Corporation
Journal of Combustion
Volume 2011, Article ID 250391, 9 pages
doi:10.1155/2011/250391

Research Article

A Comparison of Flame Spread Characteristics over Solids in Concurrent Flow Using Two Different Pyrolysis Models

Ya-Ting Tseng and James S. T'ien

Department of Mechanical and Aerospace Engineering, Case Western Reserve University, 10900 Euclid Avenue, 418 Glennan Building, Cleveland, OH 44106, USA

Correspondence should be addressed to Ya-Ting Tseng, yating@case.edu

Received 30 October 2010; Accepted 24 February 2011

Academic Editor: Kalyan Annamalai

Two solid pyrolysis models are employed in a concurrent-flow flame spread model to compare the flame structure and spreading characteristics. The first is a zeroth-order surface pyrolysis, and the second is a first-order in-depth pyrolysis. Comparisons are made for samples when the spread rate reaches a steady value and the flame reaches a constant length. The computed results show (1) the mass burning rate distributions at the solid surface are qualitatively different near the flame (pyrolysis base region), (2) the first-order pyrolysis model shows that the propagating flame leaves unburnt solid fuel, and (3) the flame length and spread rate dependence on sample thickness are different for the two cases.

1. Introduction

In modeling flame spread over solids, a description of the solid pyrolysis processes is required to complete the coupling between the gaseous flame phase and the solid phase. Typically, a pyrolysis description provides the relationship between the solid mass burning rate and the local conditions of the solid fuel being heated. The detailed chemical steps of the pyrolysis reactions, however, can be very complex, depending on the types of solids, the temperature, the heating rate, the duration, among other things. They may also vary depending on whether the surrounding atmosphere is with or without oxygen. There is an abundance of literature on the pyrolysis of materials. For example, in biomass production, a review can be found for the pyrolysis of wood and biomass [1]. Polymer pyrolysis and measurement can be found in [2]. A recent pyrolysis model intended for fire research was offered in [3].

In model computation of flame spread over solids, simplified pyrolysis reactions are needed to make the model more tractable. For example, Di Blasi [4] has employed a three-step reaction scheme: solid to vapor, solid to tar, and solid to char. A still simpler scheme is a one-step description to represent the overall solid pyrolysis conversion from solid to vapor. For cellulose, Kung [5] proposed a first-order reaction whose rate depends on the first power of the local solid density and the Arrhenius expression on temperature. This has been adopted in many opposed-flow flame spread works (e.g., [6, 7]). Because of the linear dependence on local density in the rate expression, the solid fuel is not entirely consumed in a finite length of time or in a finite distance by a spreading flame when using the first-order pyrolysis reaction model. Since some solids are observed to burn out completely in experiments, Ferkul and T'ien [8], in their concurrent flame spread model, adopted a zeroth-order pyrolysis reaction which has previously been used in solid propellant studies. The zeroth-order reaction has since been used in many subsequent works (e.g., [9, 10]).

Despite their simplicities, there are fundamental differences between the zeroth-order and the first-order pyrolysis models. The pyrolyzing mass burning rate depends only on the surface temperature in the zeroth-order model and is therefore a surface model. In the first-order model, on the other hand, pyrolysis rate depends on the local temperature and density in the interior of the solid so it is an in-depth model. Although both models have been employed in many previous flame spread computations, there is no investigation

on the differences they produce on flame spreading characteristics. This work will compare the performance of both pyrolysis expressions (zeroth- and first-order) using a detailed flame spread model over solids in a low-speed forced concurrent flow. The comparisons include flame and solid profiles, solid mass burning rate distributions, and spread rate as a function of sample thickness.

2. Theoretical Formulation

2.1. Flow and Fuel Configuration. The fuel and flow configuration considered in the mathematical model is shown in Figure 1. A spreading flame is shown schematically over a solid sample. The spread is in a two-dimensional concurrent forced flow from left to right (gravity is zero). The flame is on both sides of the sample. Because of symmetry, only one half of the flame is shown and computed. The solid of thickness τ consists of one phase of combustible (90%) and another phase of an inert matrix (10%), so that its structural integrity is retained. As the flame spreads to the right, solid residue is left behind. A uniform laminar forced air flow of magnitude V_∞ is imposed at a distance 6.3 cm upstream of the flame base. The choice of imposing the upstream flow at a fixed distance is to eliminate the variable entrance length effect since we are only interested in steady spread in this work. Experimentally it is also possible to realize a constant entrance length in spreading flames by using a special setup as demonstrated in [11]. In a previous paper, we have shown that the flame radiation feedback to the solid can reach up to 5 cm upstream [12], so the entrance length is chosen to be greater than this value. Although values other than 6.3 cm can be used, it will not alter the basic physics of the present problem.

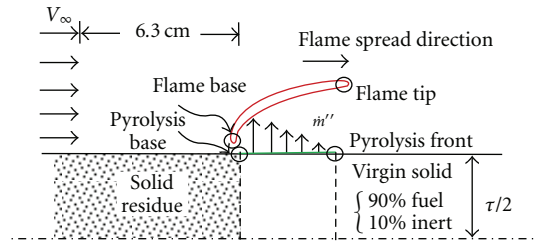

Figure 1: Configuration of a spreading flame in the computational model.

2.2. Model Description. With the exception of the pyrolysis relation, the flame spread formulation is the same as a previous model [13]. Consequently, we will only mention briefly the model details except the portion on the formulation of the pyrolysis reaction which will be dealt with more thoroughly.

Reference [13] is a transient two-dimensional model for laminar flame spread over solids in a low-speed forced concurrent flow with zero gravity. It uses an unsteady solid phase and a quasisteady gas-phase. The solid phase consists of an unsteady heat conduction equation with a zeroth-order surface pyrolysis reaction according to the Arrhenius form. The quasisteady gas-phase employs full elliptic Navier-Stokes mass and momentum equations together with energy and species equations. The species considered are fuel vapor, oxygen, CO_2, and H_2O. A one-step, second-order overall Arrhenius gas-phase reaction is adopted. Both surface and flame radiation are included. The gas-phase radiation transfer equation is solved using the S-N discrete ordinates method so that the radiation flux vectors are determined. More information on the formulation of the gas-phase processes can be found in [14].

Computations in [13] start with the ignition process. Flames grow in size initially but eventually reach steady states. For a thick solid, the steady state is a nongrowing stationary flame with a limiting length. For a thin solid, the steady state is a spreading flame with a constant spread rate and a constant flame length. The reason for a nongrowing limiting flame for the thick solid is the balance between the flame heat feedback and the surface radiative heat loss at the pyrolysis front. The reason for achieving a steady spread for thin solids is the balance between the solid burnout rate and the flame tip advancing rate. For relatively thin samples, steady spread can be obtained quickly. For thick samples, the transient growth period may dominate. Reference [15] shows that the transient pyrolysis process may affect the flame spread rate quantitatively.

In this work, we will only be interested in thin solids in the steady spreading regime. The steady regime is obtained using the transient program. Please note that, by thin solids, we refer to cases in which the upstream solid fuel burnout (or the spread of the upstream flame base) occurs within the simulation time so that the flame steady spreading state can be achieved. The thermally thin solid assumption is not imposed in this work.

2.2.1. Solid-Phase and Pyrolysis Models

(a) Zeroth-Order (Surface) Pyrolysis. For the zeroth-order pyrolysis model, the solid heat conduction equation is:

$$\frac{\partial}{\partial t}(\rho_s C_s T_s) = \frac{\partial}{\partial x}\left(k_s \frac{\partial T_s}{\partial x}\right) + \frac{\partial}{\partial y}\left(k_s \frac{\partial T_s}{\partial y}\right). \quad (1)$$

It is assumed that the solid pyrolysis occurs only on the surface and the solid fuel density $\rho_{s,F}$ remains constant during the combustion process. However, as the solid fuel is depleted, the fuel thickness τ_F decreases and hence the composition of the solid changes and the compound solid density ρ_s decreases. Until the solid fuel is completely consumed, the solid becomes pure inert (this will not happen theoretically for the first-order relation). Note also, the x-y coordinates system in (1) is fixed with respect to the laboratory. When a steady spread is achieved with a constant spread velocity V_f, (1) can be transformed into a steady form with a coordinate transformation $x' = V_f t$. So $\partial/\partial t = V_f \partial/\partial x'$.

At the interface of the solid-phase and the gas-phase, the energy conservation boundary condition is:

$$\dot{q}''_{c,\text{in}} - \dot{q}''_{r,\text{out}} - \dot{m}'' L = k_s \frac{\partial T_s}{\partial y}. \tag{2}$$

In this equation, the convective heat gain, $\dot{q}''_{c,\text{in}}$, is obtained from the quasisteady gas-phase solution, $\dot{q}''_{r,\text{out}}$, is equal to solid surface radiation heat loss minus the flame radiation feedback, and $\dot{m}'' L$ is the energy consumed in pyrolyzing the solid fuel. Note that both the left- and right-hand sides of (2) represent the net heat flux entering the interior of the solid, and thus relates to the heat-up of the solid fuel. To facilitate our discussion, we use $\dot{q}''_{\text{net,in}}$ $(= \dot{q}''_{c,\text{in}} - \dot{q}''_{r,\text{out}} - \dot{m}'' L)$ to denote this quantity.

To relate the mass burning rate to the surface temperature, a zeroth-order pyrolysis relation is assumed at the fuel surface:

$$\dot{m}'' = A_s \exp\left(\frac{-E_s}{R_u T_{s,w}}\right). \tag{3}$$

This equation indicates that the solid burning rate is very sensitive to the surface temperature for a reasonable value of E_s/R_u (i.e., $\gg 1$).

(b) First-Order (In-Depth) Pyrolysis. For the first-order in-depth pyrolysis model, the governing equation for the solid temperature has a more complex expression:

$$\begin{aligned}\frac{\partial}{\partial t}(\rho_s C_s T_s) + \frac{\partial}{\partial y}(\dot{m}'' C_s T_s) \\ = \frac{\partial}{\partial x}\left(k_s \frac{\partial T_s}{\partial x}\right) + \frac{\partial}{\partial y}\left(k_s \frac{\partial T_s}{\partial y}\right) + L\frac{\partial \rho_{s,F}}{\partial t}.\end{aligned} \tag{4}$$

In this equation, the local fuel vapor mass flux $\dot{m}''$, resulting from in-depth pyrolysis, is related to the solid fuel density decrease rate by the mass equation:

$$\frac{\partial \rho_{s,F}}{\partial t} + \frac{\partial \dot{m}''}{\partial y} = 0. \tag{5}$$

And with the first-order pyrolysis assumption, we have the following relation:

$$\frac{\partial \rho_{s,F}}{\partial t} = -A_I \rho_{s,F} \exp\left(\frac{-E_I}{R_u T_s}\right). \tag{6}$$

In this case, the local solid fuel density decreases during the burning process. The decreasing rate of $\rho_{s,F}$ is a function of itself and the local solid temperature T_s. According to (6), both $\rho_{s,F}$ and $\partial \rho_{s,F}/\partial t$ never reach zero as mentioned in the introduction.

An energy balance is imposed on the surface as the boundary condition:

$$\dot{q}''_{c,\text{in}} - \dot{q}''_{r,\text{out}} = k_s \frac{\partial T_s}{\partial y}. \tag{7}$$

Compared with (2), the latent heat loss term, $\dot{m}'' L$, is not included. It is because the solid pyrolysis is a "volumetric phenomenon" instead of a "surface phenomenon." Hence, the latent heat loss is accounted for in the energy equation (4), not in the boundary condition. The net heat flux going into the interior of the solid in this case is $\dot{q}''_{\text{net,in}} = \dot{q}''_{c,\text{in}} - \dot{q}''_{r,\text{out}}$.

The mass burning rate $\dot{m}''$ on the solid surface is one of the most important input quantities from the solid phase to the gas-phase. The fuel vapors generated beneath the surface of the solid have to transport to the surface. Here an essential approximation is made, that is, the mass transfer resistance is negligible in the direction perpendicular to the surface because of the small thickness of the solid samples. Consequently, the pyrolyzed fuel vapor inside the solid will reach the surface instantaneously and only in the direction perpendicular to the surface. This is clearly an approximation. For thicker solids, the mass transfer equation in porous media needs to be solved [16, 17]. With this assumption, (5) is integrated to obtain the mass burning rate on the solid surface for the first-order pyrolysis model:

$$\dot{m}'' = \int_0^{\tau/2} -\frac{\partial \rho_{s,F}}{\partial t} dy. \tag{8}$$

Equation (8) states that the mass burning rate (or the fuel vapor mass flux) on each side of the solid surface is the integration of the density change rate across the half solid fuel thickness $\tau/2$.

In the computations, the solid combustible properties other than density are assumed constant. They are based on cellulose. The solid combustible density $\rho_{s,F}$, remains constant in the zeroth-order pyrolysis model and varies during the combustion process in the first-order pyrolysis model. The solid combustible thermal conductivity is taken from [18] (for wood fir in the cross-grain direction). The inert matrix properties are set to be the same as those of the solid combustible for simplicity (except its density). The inert matrix density is 10% of the virgin solid density. The solid fuel properties (except A_I and E_I) can be found in [13]. The kinetics parameters for the first-order pyrolysis are $A_I = 1\times10^{10}$ 1/sec, and $E_I = 3\times10^4$ cal/mole. They are in the range of values that are quoted for thin paper samples [19].

2.3. Numerical Scheme. As mentioned earlier, steady spreading solutions are obtained by marching in time using a transient numerical code. In a laboratory-fixed x-y coordinate system, ignition occurs near $x \approx 0$. The flame base moves downstream when there is not enough fuel vapor to support the flame locally. Since the flow entrance length is fixed as discussed previously, true steady spread can be obtained. The flame structure and comparisons will be presented when the flame base is located at an x-location after the steady spread is achieved. Details of the transient processes can be found in [13].

One note on the grid size may be worthwhile. A nonuniform grid structure is adopted in this model. To resolve the flame structure in the stabilization zone (located at the flame base), the chosen characteristic length used to nondimensionalize the gas-phase equations is the thermal-diffusional distance in the flame stabilization zone, α_g/V_∞. This length is relatively large in low-speed flow. For example,

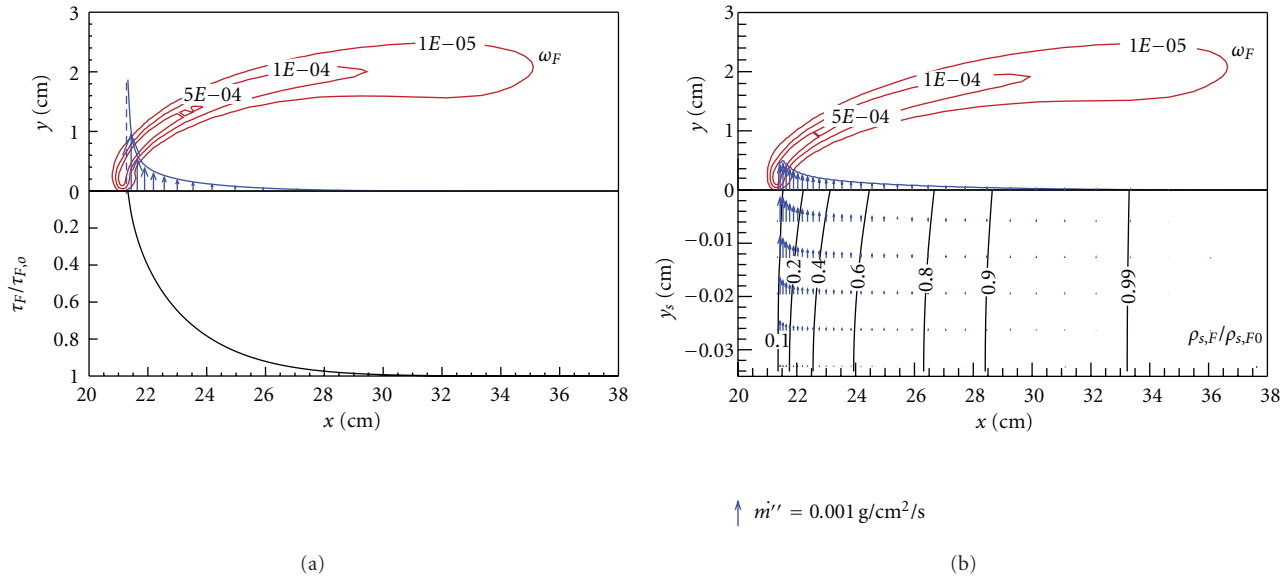

FIGURE 2: Flame structure, burning rate distribution, and the percentage of un-burnt solid at the steady state (a) with the zeroth-order pyrolysis model and (b) with the first-order pyrolysis model. Upper plane: contours of ω_F (g/cm^3 s) and $\dot{m}''$ distribution on the solid surface. Lower plane: (a) $\tau_F/\tau_{F,0}$ (b) contours of $\rho_{s,F}/\rho_{s,F0}$, and fuel vapor mass flux in the solid. Flow condition: $X_{O2,\infty} = 21\%$, $V_\infty = 5$ cm/s, and $\rho_{s,F0}\tau = 28.4$ mg/cm^2.

$\alpha_g/V_\infty = 0.426$ cm for $V_\infty = 5$ cm/s in this work. Finer grids (0.2 nondimensionalized grid size) are specified in the region close to the flame where the temperature and species gradients are large. Fine grids are also needed in the region where the flame will pass by. In the solid phase, the x-direction grids are the same as in the gas-phase. In the y-direction, uniform grids are specified. Twenty grids in y-direction are typically used. The detailed grid arrangement can be found in [13].

3. Computed Results and Discussion

Flame and solid profiles at steady spread conditions are presented and compared first. The leftover un-burnt solid fuel phenomena will be examined next. Lastly, the spread rate variations with sample thickness will be compared between the two different pyrolysis models.

3.1. Flame Structure and Solid Profiles at Steady State. In order to illustrate the differences of the flame structure between zeroth-order and first-order pyrolysis, the steady state cases with initial area density $\rho_{s,F0}\tau = 28$ mg/cm^2 are studied (except during the investigation of thickness effect). We deliberately choose this area density since the flames using both pyrolysis expressions have similar length and spread rate ($l_f = 8.55$ cm, $V_f = 0.090$ cm/s for zeroth-order pyrolysis and $l_f = 8.83$ cm, $V_f = 0.086$ cm/s for first-order pyrolysis). This facilitates the comparison of the flame and solid profiles.

3.1.1. Mass Burning Rate Distributions. The $\dot{m}''$ distribution on the solid surface is the most crucial difference between the zeroth-order and first-order pyrolysis models. As shown on the upper plane of Figure 2(a), for the zeroth-order pyrolysis, $\dot{m}''$ increases monotonically from downstream toward the flame base. It reaches the maximum value at the burnout point (where $\tau_F/\tau_{F,0} = 0$) and drops off abruptly to zero upstream. This is implied by (3) in which $\dot{m}''$ is only a function of $T_{s,w}$. $T_{s,w}$ over the pyrolysis region has a maximum value at the flame base where the flame standoff distance is the smallest. As the flame standoff distance increases, $T_{s,w}$ decreases downstream and $\dot{m}''$ decreases with $T_{s,w}$. Please note that the percentage of un-burnt solid for the surface pyrolysis case is indicated by $\tau_F/\tau_{F,0}$ which is shown on the lower plane in Figure 2(a).

The fuel vapor mass flux $\dot{m}''$ for the first-order pyrolysis case is shown as blue arrows on the lower plane in Figure 2(b). As mentioned earlier, the fuel vapor produced in-depth is assumed to convect vertically to the surface without mass transfer resistance because of the small thickness of the solid sample. The fuel vapor emerging at the solid-gas interface is the accumulation of the mass flux in-depth in the solid according to (8). Note that the resulting $\dot{m}''$ on the solid surface shown on the upper plane of Figure 2(b) is very different from that of the zeroth-order pyrolysis model. There is no abrupt cutoff and the maximum value occurs downstream of the pyrolysis base. Instead, $\dot{m}''$ reaches a maximum (much smaller than that in the zeroth-order case) and then decreases toward zero. This is because in the first-order pyrolysis model, the local burning rate is not only function of local temperature but also local solid fuel density. Although T_s is higher near the pyrolysis base, the lower $\rho_{s,F}$ results in a smaller burning rate. The $\rho_{s,F}/\rho_{s,F0}$ contours are also shown on the lower plane of Figure 2(b) for reference. This different shape of the $\dot{m}''$ distribution on the solid

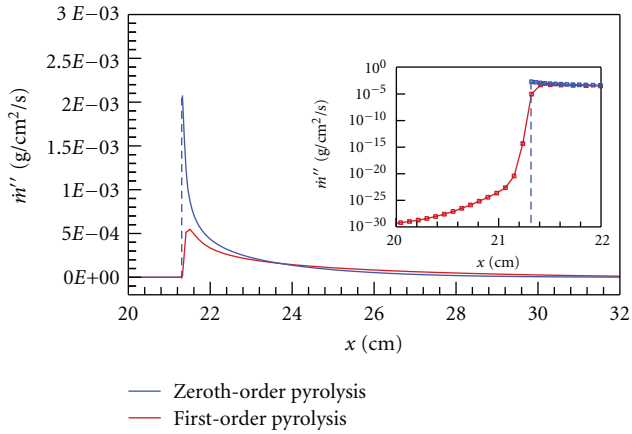

FIGURE 3: Fuel vapor mass flux, $\dot{m}''$ distributions on the solid surface for both pyrolysis models. In the inset, a log-scale ordinate is use d.

surface for the first-order pyrolysis model results in some interesting phenomena which will be discussed later.

The different distributions of the surface $\dot{m}''$ between the two pyrolysis models just discussed are highlighted in the comparison in Figure 3. The total burning rate, $\dot{m}'$ (the integration of $\dot{m}''$ over the solid surface) of both cases are very close (1.35×10^{-3} g/cm/s for surface pyrolysis and 1.22×10^{-3} g/cm/s for in-depth pyrolysis). This is expected since these two cases have the same area density and similar spread rates (one can refer to (9) which will be presented later). Although $\dot{m}''$ for the first-order pyrolysis case has a smaller value near the pyrolysis base region (where the un-burnt solid percentage is smaller), it trails longer downstream and has a larger value than that in the zeroth-order pyrolysis model after $x > 23.5$ cm. Also, $\dot{m}''$ will not reach zero inside the flame zone according to our discussion in the introduction. A log-scale ordinate is used to demonstrate this phenomenon in the inset.

3.1.2. Flame Structures. In order to illustrate the flame structures, gas-phase reaction rate ω_F and flame temperature contours are shown on the upper plane of Figures 2 and 4, respectively. Although the flame lengths (defined here by $\omega_F = 10^{-4}$ g/cm^3 s) of these two models are very close, the flame structures are very different. The contours of ω_F in Figure 2 indicate that the reaction is more vigorous near the flame base region for the zeroth-order pyrolysis case. If one compares the contours of ω_F at a higher value, say 5×10^{-4} g/cm^3 s, one would notice that the zeroth-order pyrolysis case has a longer flame length (3.0 cm versus 2.3 cm). Also, the maximum value of ω_F for the zeroth-order pyrolysis model is a bit higher than that of the first-order pyrolysis model ($\omega_{F,\max} = 1.6 \times 10^{-3}$ g/cm^3 s and 1.5×10^{-3} g/cm^3 s for each model, resp.). However, if one compares contours of ω_F at a smaller value, say 10^{-5} g/cm^3 s, the first-order pyrolysis model has the longer contour length (14.4 cm versus 15.6 cm). This is the results of the different $\dot{m}''$ distributions between the two models. Using the zeroth-order pyrolysis model, $\dot{m}''$ is concentrated near the flame

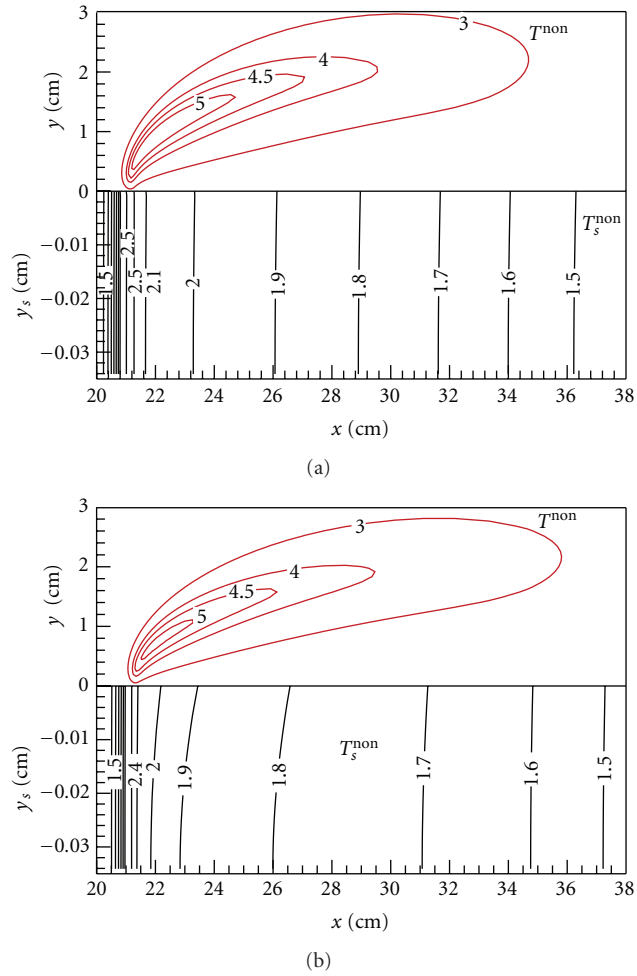

FIGURE 4: Temperature profiles of the gaseous flame and the solid phase at the steady state (a) with the zeroth-order pyrolysis model and (b) with the first-order pyrolysis model. Upper plane: nondimensional gas-phase temperature contours. Lower plane: nondimensional solid-phase temperature contours. Temperature is nondimensionalized by 300 K. Ordinate scales are different in y (gas-phase) and y_s (solid phase).

base region and has a larger maximum value. On the other hand, $\dot{m}''$ for the first-order pyrolysis case is more distributed along the solid surface.

The temperature contours in Figure 4 further illustrate the flame structures of both cases. Similarly, if one compares contours of the nondimensional value 4, both models give a similar contour length. But one would find the zeroth-order pyrolysis model has a longer contour length by comparing contours of a larger value and a shorter contour length by comparing contours of a smaller value.

3.1.3. Heat Fluxes on the Solid Surface. As discussed earlier, these two pyrolysis models have a different energy balance on the solid surface (refer to (2) and (7)). Heat flux distributions on the solid surface for both models are shown in Figure 5. In this figure, the convective heat flux, $\dot{q}''_{c,\text{in}}$ (red line) and the net radiative loss from the surface, $\dot{q}''_{r,\text{out}}$ (green line)

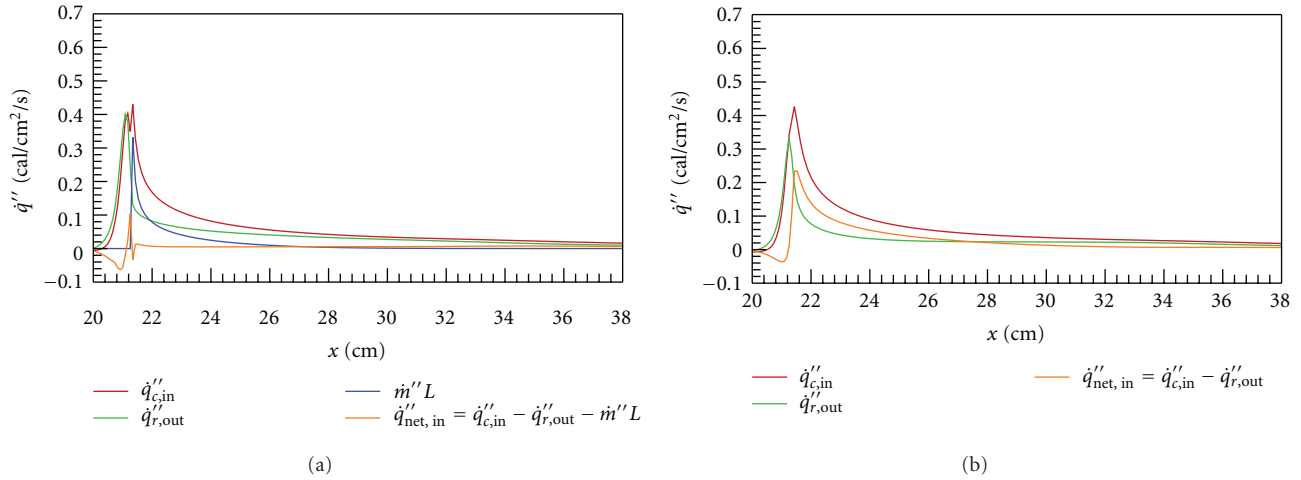

FIGURE 5: Heat fluxes on solid surface at the steady state (a) with the zeroth-order pyrolysis model and (b) with the first-order pyrolysis model.

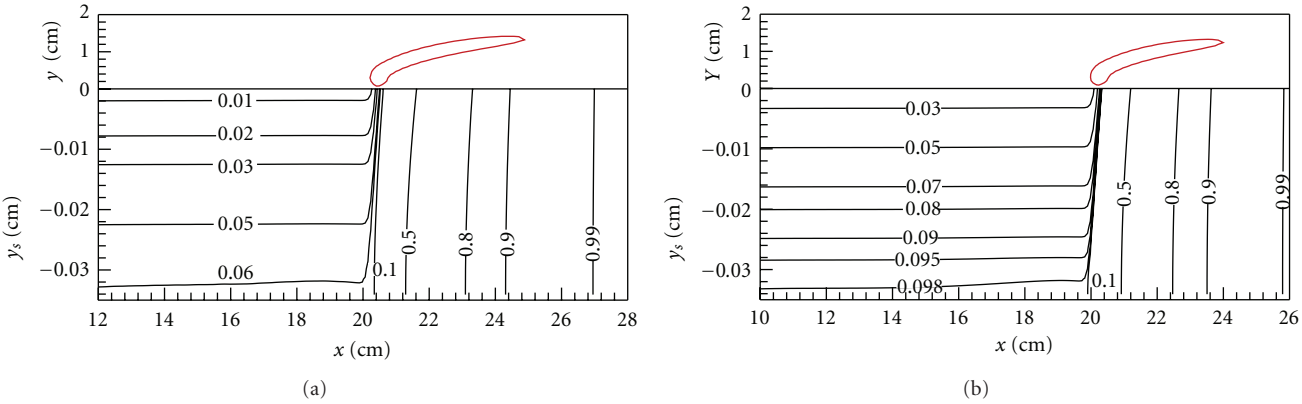

FIGURE 6: Solid leftover occurs when flames are near the extinction limit. (a) $X_{O2,\infty} = 16\%$ (b) $X_{O2,\infty} = 15\%$. Upper plane: indication of visible flame shape. Lower plane: solid residual fuel percentage. (contours of $\rho_{s,F}/\rho_{s,F0}$). Ordinate scales are different in y (gas-phase) and y_s (solid phase).

have the same features for both models. However, the net heat fluxes going into the interior of the solid, $\dot{q}''_{\text{net,in}}$ (orange line), are very different. For the zeroth-order case, $\dot{q}''_{\text{net,in}}$ is very close to zero over the entire pyrolysis region as shown in Figure 5(a). It is because surface pyrolysis takes place and consumes the energy from the flame. Please note that $\dot{q}''_{\text{net,in}}$ has a small finite value around the pyrolysis front which preheats the solid fuel and enables the flame to spread downstream. This phenomenon is discussed in a previous paper [13]. The solid temperature profile is shown in Figure 4(a). It is shown that the solid fuel is thermally thin in this case.

In comparison, the heat flux from the gas-phase ($\dot{q}''_{\text{net,in}}$) for the first-order pyrolysis case, is not consumed on the surface. It goes into the solid interior while being balanced by the local solid pyrolysis. This positive $\dot{q}''_{\text{net,in}}$ explains the nonuniform solid temperature along the solid thickness as shown in Figure 4(b). In the region $21\,\text{cm} < x < 27\,\text{cm}$, there is substantial nonzero $\dot{q}''_{\text{net,in}}$ as shown in Figure 5(b). One can notice the solid temperature contours in the same region (Figure 4(b)) bent a little bit, reflecting that the solid is heated up by the energy from the gas-phase in additional to the streamwise heat conduction within the solid phase.

3.2. Solid Fuel Leftover Phenomenon. Another difference between two solid pyrolysis cases observed in this work is the phenomenon of the solid fuel leftover after flame-passage in the first-order pyrolysis model. In the zeroth-order pyrolysis case, the maximum of $\dot{m}''$ is located at the solid burnout point which makes the flame base anchor near the burnout point. The flame only spreads downstream when the solid fuel is completely consumed. Solid fuel leftover can never be observed in the steady spreading state according to the zeroth-order pyrolysis model. On the other hand, leftover solid fuel is found using the first-order pyrolysis model. This can be numerically visualized most easily in the near-limit flames. In this work, the near-limit regime is reached by lowering the ambient oxygen percentage, $X_{O2,\infty}$.

To approach the extinction limit, $X_{O2,\infty}$ is lowered from 21%. When $X_{O2,\infty} = 16\%$, Figure 6(a) gives a snapshot of

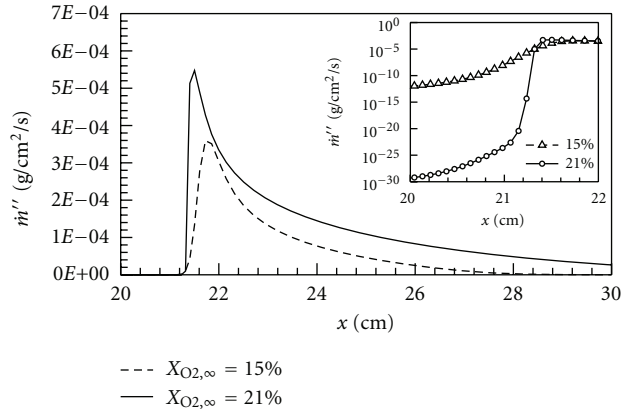

FIGURE 7: Fuel vapor mass flux $\dot{m}''$ distribution on the solid surface changes when the flame approaches the extinction limit for the first-order pyrolysis cases. In the inset, a log-scale ordinate is used.

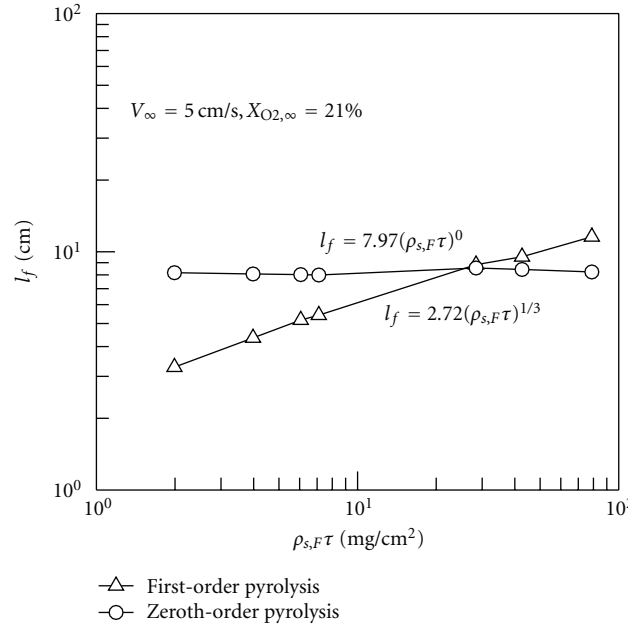

FIGURE 8: Thickness effect on flame length for both pyrolysis models.

the solid residual percentage (shown on the lower plane) after the flame reaches the steady spreading state. The visible flame is also shown on the upper plane. The flame is ignited at $x = 0$, propagates downstream, reaches steady state, and leaves the same amount of solid fuel unburned upstream. In this snapshot, the flame base has spread to $x = 20$ cm and 6% of the solid fuel is left near the centerline of the solid. Figure 6(b) shows even more leftover solid fuel (around 10% near the centerline) is observed when $X_{O2,\infty}$ is further lowered to 15%. This phenomenon can be explained by the nature of the $\dot{m}''$ distribution. Figure 7 shows $\dot{m}''$ on the solid surface of the steady flame at $X_{O2,\infty} = 15\%$ along with that at $X_{O2,\infty} = 21\%$. One can notice that not only does the peak value decrease, but the peak location shifts downstream a bit as well. When there is not enough fuel vapor supporting the local reaction, the flame base will move downstream seeking more fuel vapor due to finite rate kinetics (remember that the peak value of $\dot{m}''$ occurs downstream to the pyrolysis base). In this situation, the flame might spread downstream before the solid fuel burns out completely. The weaker the flame, the greater the downstream shift of the $\dot{m}''$ peak and the higher the percentage of solid fuel left un-burnt. The inset in Figure 7 shows as the flame weakens, the drop of $\dot{m}''$ toward upstream becomes more gradual. More gradual drop is also expected if the activation energy of the first-order pyrolysis reaction is lowered.

3.3. Sample Thickness Effect

3.3.1. Thickness Effect on Flame Length. Another difference between these two pyrolysis models is how the steady flame responds to the different solid sample thicknesses (or sample area density). Within the investigated thickness regime, the gaseous flames are essentially the same for different $\rho_{s,F}\tau$ in the surface pyrolysis model, which is reasonable. As mentioned earlier, $\dot{m}''$ is only a function of $T_{s,w}$ in the zeroth-order pyrolysis assumption. Therefore, with approximately the same pyrolysis temperature, $\dot{m}''$ is the same regardless of $\rho_{s,F}\tau$. As shown in Figure 8, the steady flame length l_f is almost constant for different $\rho_{s,F}\tau$ in the zeroth-order pyrolysis model.

On the other hand, as suggested by (6) and (8), burning rate on the surface for first-order pyrolysis increases with the solid thickness (again, by assuming the pyrolysis temperature is very close for different $\rho_{s,F}\tau$ cases). As a result, l_f at steady state increases with the $\rho_{s,F}\tau$ as shown in Figure 8. For this case, the l_f dependence on $\rho_{s,F}\tau$ is of power 1/3 ($l_f \propto (\rho_{s,F}\tau)^{1/3}$).

3.3.2. Thickness Effect on Spread Rate. One of the important features of a spreading flame over a solid is the spread rate. When the steady state is reached, by the conservation of solid fuel mass, one can have the following equation (neglecting fuel leftover):

$$V_f \rho_{s,F}\tau = \dot{m}'. \tag{9}$$

The computed results show that the total burning rate, $\dot{m}'$ is proportional to the flame length, l_f. Therefore, the V_f dependence on $\rho_{s,F}\tau$ can be expressed as follows:

$$V_f = \frac{\dot{m}'}{\rho_{s,F}\tau} \propto \frac{l_f}{\rho_{s,F}\tau} \propto (\rho_{s,F}\tau)^{a-1}, \tag{10}$$

where a is the power dependence of l_f on $\rho_{s,F}\tau$ discussed previously: $a \approx 0$ for the zeroth-order pyrolysis model and $a \approx 1/3$ for the first-order pyrolysis model. V_f versus $\rho_{s,F}\tau$ for both solid pyrolysis models are shown in Figure 9. It is not surprising that the theoretical prediction of the power dependence of V_f on $\rho_{s,F}\tau$ coincides nicely with the numerical results, -1 and $-2/3$ for the zeroth-order pyrolysis model and the first-order pyrolysis model, respectively, as shown in the figure.

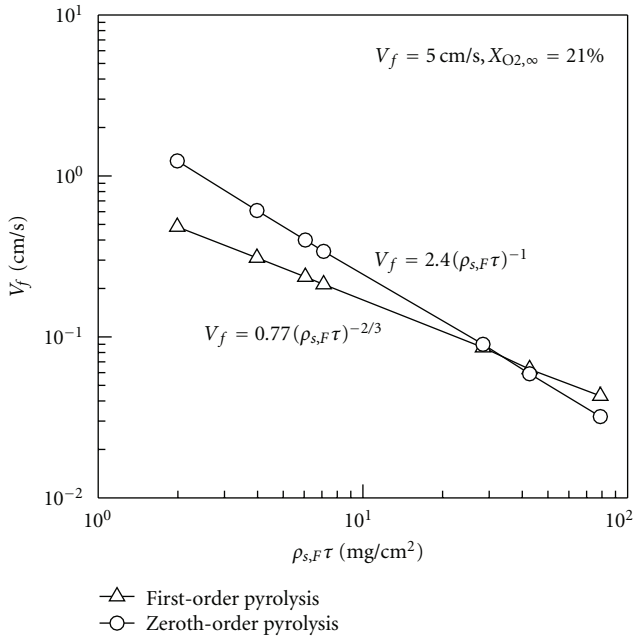

Figure 9: Thickness effect on spread rate for both pyrolysis models.

4. Conclusions

Using a two-dimensional, transient, laminar flame spread code, computed steady spreads over thin solids in low-speed concurrent forced flow have been obtained using two different solid pyrolysis models. Comparisons of the numerical results show many differences between the zeroth-order surface pyrolysis and the first-order in-depth pyrolysis cases. The following are some of the key findings of this work.

(1) The mass burning rate distributions on the solid surface are qualitatively different. For the zeroth-order pyrolysis, solid pyrolysis occurs on the solid surface only and the fuel vapor mass flux on the surface reaches a maximum value at the fuel burnout point with an abrupt drop to zero upstream. For the first-order pyrolysis, solid decomposition occurs everywhere within the solid fuel once being heated. The fuel mass flux on the surface is the accumulation of the local vapor produced inside the solid. The peak of fuel mass flux on the surface occurs in the pyrolysis region. It will not drop to zero within the finite domain of the flame zone.

(2) The nature of the fuel mass flux distribution results in a special leftover fuel phenomenon which is not observed in the zeroth-order pyrolysis model. Due to finite rate gas-phase reaction used in the model, the flame base will adjust its location to find enough fuel vapor. In the zeroth-order pyrolysis model, the flame base always anchors at the solid burnout point where fuel mass flux has the maximum value. On the other hand, in the first-order pyrolysis model, the peak value of fuel mass flux becomes smaller and its location shifts downstream when the flame approaches the extinction limit. The flame base moves before solid fuel burns out completely thus leaving unburned solid fuel upstream.

(3) Solid fuel thickness effects on the flame length and the spread rate for each pyrolysis model are also different. In the zeroth-order pyrolysis model, gaseous flames are essentially the same for different sample thicknesses. The flame length is independent of thickness and the spread rate is approximately inversely proportional to thickness. In the first-order in-depth pyrolysis model, fuel mass flux at the surface increases with thickness, resulting in a longer flame. The computed result shows that flame length increases with thickness with a power dependence of 1/3. The spread rate decreases with thickness with a $-2/3$ power dependence.

The present numerical results show that different solid pyrolysis models can have a drastic influence on flame spreading behavior in concurrent flow. Their effect on opposed-flow spread is not yet clear. More sophisticated pyrolysis models also need to be tested in the future to assess their influence.

Nomenclature

a: Power dependence of the flame length on the sample thickness
A_I: Solid-phase preexponential factor for the in-depth pyrolysis model
A_s: Solid-phase preexponential factor for the surface pyrolysis model
C_s: Solid-phase-specific heat
E_I: Solid-phase activation energy for the in-depth pyrolysis model
E_s: Solid-phase activation energy for the surface pyrolysis model
k_s: Solid-phase-specific heat
L: Latent heat
l_f: Flame length
$\dot{m}'$: Total mass burning rate total (the integration of $\dot{m}''$ over the solid surface)
$\dot{m}''$: Mass burning rate or fuel vapor mass flux
$\dot{q}''_{c,\,\mathrm{in}}$: Convective heat flux on the solid surface from the gas-phase
$\dot{q}''_{r,\mathrm{out}}$: Net radiative heat loss from the solid surface
$\dot{q}''_{\mathrm{net,in}}$: Net heat flux going into the interior of the solid $(= \dot{q}''_{c,\mathrm{in}} - \dot{q}''_{r,\mathrm{out}} - \dot{m}''L)$
R_u: Universal gas constant
t: Time
T_s: Solid temperature
$T_{s,w}$: Solid surface temperature
V_f: Flame spread rate
V_∞: Free stream velocity
$X_{O2,\infty}$: Free stream oxygen molar fraction
x: x-coordinate
x': Transformed x-coordinate

y: y-coordinate
y_s: y-coordinate for the solid phase
α_g: Gas-phase thermal diffusivity
ρ_s: Compound solid density
$\rho_{s,F}$: Solid fuel density
$\rho_{s,F0}$: Initial solid fuel density
τ: Virgin sample thickness
τ_F: Solid fuel thickness
$\tau_{F,0}$: Initial solid fuel thickness
ω_F: Fuel vapor consumption rate
$\omega_{F,\max}$: Maximum fuel vapor consumption rate at a certain instant.

Acknowledgment

This research is supported by a grant from NASA Glenn Research Center monitored by Dr. Gary Ruff.

References

[1] D. Mohan, C. U. Pittman, and P. H. Steele, "Pyrolysis of wood/biomass for bio-oil: a critical review," *Energy and Fuels*, vol. 20, no. 3, pp. 848–889, 2006.

[2] R. E. Lyon and R. N. Walters, "Pyrolysis combustion flow calorimetry," *Journal of Analytical and Applied Pyrolysis*, vol. 71, no. 1, pp. 27–46, 2004.

[3] C. Lautenberger and C. Fernandez-Pello, "Generalized pyrolysis model for combustible solids," *Fire Safety Journal*, vol. 44, no. 6, pp. 819–839, 2009.

[4] C. Di Blasi, "Processes of flames spreading over the surface of charring fuels: effects of the solid thickness," *Combustion and Flame*, vol. 97, no. 2, pp. 225–239, 1994.

[5] H. C. Kung, "A mathematical model of wood pyrolysis," *Combustion and Flame*, vol. 18, no. 2, pp. 185–195, 1972.

[6] A. E. Frey and J. S. T'ien, "A theory of flame spread over a solid fuel including finite-rate chemical kinetics," *Combustion and Flame*, vol. 36, pp. 263–289, 1979.

[7] S. Bhattacharjee and R. A. Altenkirch, "Radiation-controlled, opposed-flow flame spread in a microgravity environment," *Proceeding of Combustion Institute*, vol. 23, no. 1, pp. 1627–1633, 1991.

[8] P. V. Ferkul and J. S. T'ien, "A model of low-speed concurrent flow flame spread over a thin fuel," *Microgravity Science and Technology*, vol. 99, no. 4–6, pp. 345–370, 1994.

[9] C. B. Jiang, J. S. Tien, and H. Y. Shih, "Model calculation of steady upward flame spread over a thin solid in reduced gravity," *Proceeding of Combustion Institute*, vol. 26, no. 1, pp. 1353–1360, 1996.

[10] H. Y. Shih and J. S. T'ien, "A three-dimensional model of steady flame spread over a thin solid in low-speed concurrent flows," *Combustion Theory and Modelling*, vol. 7, no. 4, pp. 677–704, 2003.

[11] P. Ferkul, J. Kleinhenz, H. Y. Shih, R. Pettegrew, K. Sacksteder, and J. T'ien, "Solid fuel combustion experiments in microgravity using a continuous fuel dispenser and related numerical simulations," *Microgravity Science and Technology*, vol. 15, no. 2, pp. 3–12, 2004.

[12] A. Kumar, H. Y. Shih, and J. S. T'ien, "A comparison of extinction limits and spreading rates in opposed and concurrent spreading flames over thin solids," *Combustion and Flame*, vol. 132, no. 4, pp. 667–677, 2003.

[13] Y.-T. Tseng and J. S. T'ien, "Limiting length, steady spread and non-growing flames in concurrent flow over solids," *Journal of Heat Transfer*, vol. 132, no. 9, Article ID 091201, 2010.

[14] J. S. T'ien, H.-Y. Shih, C.-B. Jiang et al., "Mechanisms of flame spread and smolder wave propagation," in *Microgravity Combustion: Fire in Free Fall*, pp. 299–418, Academic Press, San Diego, Calif, USA, 2001.

[15] M. M. Delichatsios and M. A. Delichatsios, "Effects of transient pyrolysis on wind-assisted and upward flame spread," *Combustion and Flame*, vol. 89, no. 1, pp. 5–16, 1992.

[16] J. S. T'Ien and M. P. Raju, "Two-phase flow inside an externally heated axisymmetric porous wick," *Journal of Porous Media*, vol. 11, no. 8, pp. 701–718, 2008.

[17] H. R. Baum and A. Atreya, "A model of transport of fuel gases in a charring solid and its application to opposed-flow flame spread," in *31st International Symposium on Combustion*, pp. 2633–2641, deu, August 2006.

[18] A. I. Brown and S. M. Marco, *Introduction to Heat Transfer*, McGraw-Hill, New York, NY, USA, 3rd edition, 1958.

[19] P. C. Lewellen, W. A. Peters, and J. B. Howard, "Cellulose pyrolysis kinetics and char formation mechanism," in *Proceedings of the 16th International Symposium on Combustion*, pp. 1471–1480, 1977.